Bulletin of Mathematical Biology (2010) 72: 1464–1491
DOI 10.1007/s11538-010-9504-9

ORIGINAL ARTICLE

Multiscale Modelling of Fluid and Drug Transport in Vascular Tumours

Rebecca J. Shipley*, S. Jonathan Chapman

Mathematical Institute, 24-29 St. Giles, Oxford OX1 3LB, UK

Received: 8 June 2009 / Accepted: 7 January 2010 / Published online: 23 January 2010

Abstract A model for fluid and drug transport through the leaky neovasculature and porous interstitium of a solid tumour is developed. The transport problems are posed on a micro-scale characterized by the inter-capillary distance, and the method of multiple scales is used to derive the continuum equations describing fluid and drug transport on the length scale of the tumour (under the assumption of a spatially periodic microstructure). The fluid equations comprise a double porous medium, with coupled Darcy flow through the interstitium and vasculature, whereas the drug equations comprise advection–reaction equations; in each case the dependence of the transport coefficients on the vascular geometry is determined by solving micro-scale cell problems.

Keywords Homogenization · Vascular network

1. Introduction

The success of anticancer therapies in treating cancer is limited by their inability to reach their target *in vivo* in adequate quantities (Jain, 1989). If anti-cancer drugs are unable to access all of the cells within a tumour that are capable of regeneration, their effectiveness will be compromised. In addition, the effectiveness of new molecular medicines at treating cancer will be jeopardized if they cannot reach all cancerous cells (Minchinton and Tannock, 2006). An agent that is delivered intravenously reaches cancer cells via distribution through the vasculature, transport across the walls of the vessels that comprise the capillary bed, and transport through the interstitium. Each of these involves a combination of advection and diffusion, and in addition a molecule may bind to proteins or targets, be metabolized, or be retained in tumour cells.

The blood network structure of a tumour is clearly an important component of the drug delivery process. To obtain nutrients for growth, tumours sprout new blood vessels in a process called angiogenesis (Cameliet and Jain, 2000). The resulting vasculature exhibits high structural and functional heterogeneity. Blood vessels in tumours are substantially

*Corresponding author.
E-mail address: shipley@maths.ox.ac.uk (Rebecca J. Shipley).

leakier than in healthy tissue (Hashizume et al., 2000) and are tortuous, causing spatial and temporal heterogeneity in tumour blood flow. Further, the pressure generated by proliferating cells reduces tumour blood and lymphatic flow (Jang et al., 2003). Collectively, these vascular abnormalities lead to an impaired blood supply and abnormal tumour microenvironment characterized by hypoxia and elevated interstitial fluid pressure that reduces the distribution of macromolecules through advection (Heldin et al., 2004). Drug treatments (mainly anti-angiogenics such as avastin, but also vascular disrupting and regularising agents such as combretastatin and nelfinavir) have been developed specifically to target the abnormal vasculature in tumours; however, their impact is hard to predict as the relationship between network structure and the functional parameters that determine mass transport is subtle. For example, increasing the number or diameter of vessels can impair the blood flow distribution, whilst inhibiting angiogenesis is hypothesized to improve circulation (Pries et al., 2009).

In recent years, imaging techniques have advanced significantly and it is now possible to describe vascular structure in a highly detailed way (see, for example Konerding et al., 1999, 2001). As the resolution of this data continues to increase, it will become too computationally intensive to simulate flow and mass transport in the entire vascular tree using a discrete approach. Therefore, continuum models must be developed that use this imaging data as model inputs to deduce functional properties relevant to blood and mass transport.

Here, we develop a continuum model for fluid and drug transport in vascularized tumours by extending the homogenization approach of Chapman et al. (2008) to account for an arbitrary (periodic) vascular geometry. The goal of this approach is to develop a concrete mathematical framework in which to derive continuum models of fluid and mass transport in tumours. In the long-term, this will help to both elucidate the mechanisms underlying transport, and to quantify the impact of vascular structure on tumour-scale fluid and drug perfusion. As a first step in this process, this paper is focussed on model development under a number of simplifying assumptions. In particular, we model the vasculature as a highly interconnected capillary bed with a spatially periodic microstructure. This enables continuum equations for the fluid pressures and drug concentrations on the tumour-scale to be derived using the process of multiple scales. Although this approach does not account for several key features of the tumour vasculature (in particular a temporally evolving structure that may not be spatially periodic, and the hierarchical structure of the vascular tree), it does provide a methodical and mathematically solid foundation for future studies and model development. The final continuum equations are computationally tractable, and will enable the impact of varying vascular structure on tumour-scale fluid perfusion and mass transport to be tested, without re-deriving the models each time.

In Section 2, we formulate and non-dimensionalize the fluid and drug transport models on a length scale characterized by the inter-capillary separation. This includes a detailed discussion of parameter values and scalings for the dimensionless parameters that characterize the transport problems. For drug transport, we categorize the possibilities into five different transport problems, dependent on the relative importance of advection, diffusion, and reaction, and the treatment of the capillary-interstitium boundary. In Section 3, we use multiple scales to derive the continuum equations describing the fluid and drug transport on the length scale of the tumour. The resulting fluid transport model is similar to that described in Chapman et al. (2008), in that it comprises a double porous medium with coupled Darcy flow through the interstitium and vasculature; however, this approach

generalizes the grid capillary geometry of Chapman et al. (2008) to an arbitrary periodic structure. Similarly, analytic expressions for the effective drug transport coefficients are determined, and the dependence of these on the vascular geometry and drug type is highlighted. Finally, in Section 6, we present our conclusions.

2. Model formulation

The capillaries of a tumour are embedded in the interstitium (comprised of cells and extra-cellular space) and are relatively small compared to the size of the tumour domain itself. Therefore, we characterize the problem by two length scales; the macro- (or global) scale of the tumour and the micro- (or local) scale characterized by the inter-capillary separation, and on which individual capillaries are identifiable. Denoting typical tumour and inter-capillary length scales by L and d respectively, we assume that the macro- and micro- scales are well separated so that

$$\varepsilon = \frac{d}{L} \ll 1, \tag{1}$$

and exploit this in the asymptotic analysis that follows. We assume the tumour can be described as spatially periodic on the micro-scale, and consists of distinct vascular and interstitial (or tissue) phases. On the micro-scale, the medium is denoted $\Omega \subset \mathcal{R}^3$ and is composed of a porous interstitial part, Ω_t, and a capillary network region, Ω_c. The interface between the two regions (the capillary wall) is denoted $\Gamma = \partial\Omega_t \cap \partial\Omega_c$.

The assumption of a periodic microstructure was discussed in the Introduction. Although it is a simplifying assumption for tumours (and should be relaxed in future work), it enables multiple scales to be used to derive the macro-scale equations, and in this way allows a concrete mathematical framework to be developed under which fluid and mass transport can be explored. A 2D schematic of the micro- and macro-scales is depicted in Fig. 1, for an example periodic unit. On the right-hand side of Fig. 1 is the macro- (or global) scale of the tumour. On this length scale, both the vasculature and interstitium are averaged out and can be represented as continua; therefore, the distribution of fluid and drugs in each of the phases can be represented as a 'grey-scale'. In contrast, 'zooming' into a point on the macro-scale reveals the micro-scale where both the vessels and interstitium are identifiable. Circled is a schematic of a single periodic unit that repeats to form the tumour. Although the structure must be periodic, there is no other assumption of homogeneity within this unit.

Next, we consider the fluid and drug transport problems in turn.

2.1. Fluid transport

We denote the fluid velocity by $\mathbf{u}$ and the pressure by p. We denote the restriction to Ω_t or Ω_c by the subscript t or c respectively. We assume that the flow in both the interstitium and the capillaries is incompressible. The interstitium is comprised of cells surrounded by extra-cellular space. However, the capillaries are much larger than the pore size of the interstitium (i.e. the inter-cell separation), and so we treat the interstitium as an isotropic porous medium and describe fluid flow through it by Darcy's law. Therefore,

$$\nabla \cdot \mathbf{u}_t = 0 \quad \text{in } \Omega_t, \tag{2}$$

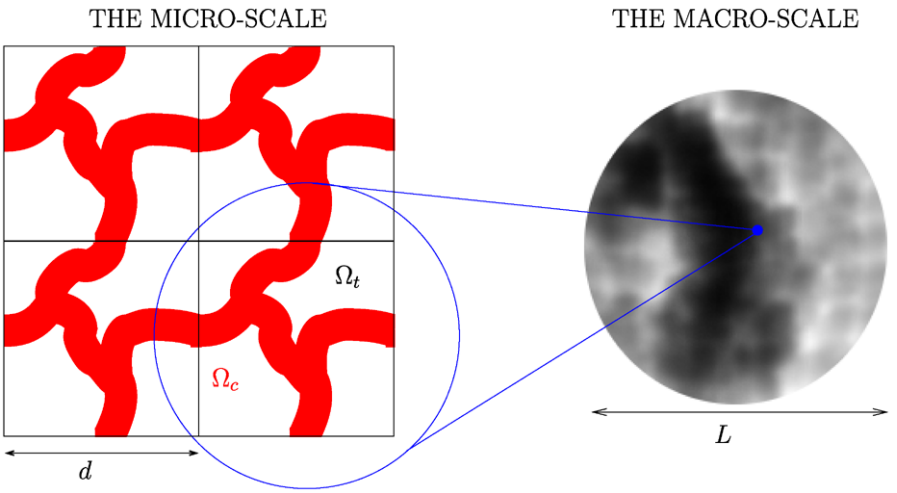

Fig. 1 A 2D schematic of the micro- and macro-scales. On the right-hand side is the macro-scale, where the vasculature and interstitium are continua and the distribution of fluid and drugs in each of the phases can be represented as a 'grey-scale'. 'Zooming' (represented in blue) into a point on the macro-scale reveals the micro-scale where both the vessels and interstitium are identifiable. The blue circled region is an example of a periodic unit. (Colour figure online.)

$$\mathbf{u}_t = -\frac{k}{\mu}\nabla p_t \quad \text{in } \Omega_t, \tag{3}$$

where k is the interstitial permeability and μ is the viscosity of the fluid.

Blood flow in the capillaries of the microcirculation is a highly complex process. Healthy human blood is a concentrated suspension containing red blood cells (RBCs) at a concentration (haematocrit) of 40–45%. In vessels much larger than the RBCs (i.e. with diameter much larger than $\approx$8 μm), blood can be treated as a continuum with a viscosity that is approximately constant. In vessels smaller than this, the finite size of RBCs results in non-continuum behaviour and complex rheology that causes several important effects, e.g. the Fåhraeus (Fåhraeus, 1928) and Fåhraeus–Lindqvist (Fåhraeus and Lindqvist, 1931; Pries et al., 1992) effects, and phase separation at diverging bifurcations (Pries et al., 1989; Pries and Secomb, 2005).

For simplicity, and with a view to elucidating the homogenization technique, we neglect non-Newtonian effects here and assume that the fluid flow in the capillaries is described by the Navier–Stokes equations for a fluid of constant viscosity. This is a significant simplifying assumption that should be addressed in future work. We have

$$\nabla \cdot \mathbf{u}_c = 0 \quad \text{in } \Omega_c, \tag{4}$$

$$\rho\left(\frac{\partial \mathbf{u}_c}{\partial t} + (\mathbf{u}_c \cdot \nabla)\mathbf{u}_c\right) = -\nabla p_c + \mu\nabla^2\mathbf{u}_c \quad \text{in } \Omega_c, \tag{5}$$

where ρ is the fluid density.

The leakage from the capillaries into the interstitium is given by Starling's law,

$$\mathbf{q}_e = L_p(p_c - p_t)\mathbf{n}, \tag{6}$$

where $\mathbf{q}_e$ is the leakage flux, L_p is the vascular permeability (assumed constant), $\mathbf{n}$ is the unit outward pointing normal to the capillary surface, and p_c, p_t are evaluated on the interior and exterior sides of the capillary wall, respectively. Given this, we impose continuity of mass flux across Γ, so that

$$\mathbf{u}_t \cdot \mathbf{n} = \mathbf{u}_c \cdot \mathbf{n} = L_p(p_c - p_t) \quad \text{on } \Gamma. \tag{7}$$

Equations (7) are enough to determine the velocity in the tissue, but Eq. (5), being of higher order, requires a further boundary condition on (for example) the tangential components of $\mathbf{u}$. Beavers and Joseph (1967) were the first to consider the appropriate form of the boundary condition for the tangential component of the velocity when a Newtonian fluid flows over a porous membrane by conducting experiments based on a 2D flow in a channel over a naturally permeable block, under an imposed pressure gradient. They concluded that a free fluid in contact with a porous medium flows faster than a fluid in contact with a completely solid surface, and a small boundary layer develops near the interface within which the tangential velocity of the fluid does not vanish. Saffman justified the Beavers and Joseph boundary condition theoretically in his paper (Saffman, 1971) by using a statistical approach to extend Darcy's law to non-homogeneous porous medium. Jones extended their result to curved boundaries and non-tangential flows (Jones, 1973), by deriving the boundary condition

$$\left[(\mathbf{n} \cdot \nabla)\mathbf{u}_c\right] \cdot \boldsymbol{\tau} = -\frac{\alpha}{\sqrt{k}}\mathbf{u}_c \cdot \boldsymbol{\tau} \quad \text{on } \Gamma, \tag{8}$$

where $\boldsymbol{\tau}$ is a unit tangential vector to Γ, and α is a dimensionless constant depending on the properties of the interface.

In practice, slip at the capillary surface will be determined by the microvascular rheology, in particular the structure of the endothelial glycocalyx. Given that we have neglected non-Newtonian effects here, we use Jones' boundary condition (8) to account for slip under the assumption that α will be determined by rheological effects. It should be noted that the boundary condition (8) has only been derived in 2D, and the extension to 3D is non-trivial (Jäger and Mikelić, 2000; Jäger et al., 2001). Here, we assume that (8) holds for both of the tangent vectors to the vascular surface.

2.2. *Drug transport*

We denote the species concentration by c, with subscripts t and c denoting the restriction to Ω_t and Ω_c respectively. We consider the transport of an arbitrary macromolecule that is advected by the fluid and diffuses in all of Ω. In addition, the species may decay/be metabolised in the interstitium, and so the transport problem may be described by

$$\frac{\partial c}{\partial t} + (\mathbf{u} \cdot \nabla)c = D\nabla^2 c - \Lambda c \quad \text{in } \Omega, \tag{9}$$

where D is the species diffusivity, assumed constant in each region (and denoted D_t and D_c in Ω_t and Ω_c, respectively), and

$$\Lambda = \begin{cases} 0 & \text{in } \Omega_c, \\ \lambda & \text{in } \Omega_t, \end{cases} \tag{10}$$

where λ represents the rate of species loss due to decay, cellular uptake, protein-mediated uptake and metabolism in the interstitium. We have assumed that this rate of species loss is proportional to the underlying drug concentration; this is a simplification, and indeed the analysis that follows could be extended to more complex reaction mechanisms in the future.

Finally, we consider the boundary conditions on the blood-interstitium boundary, Γ. Conservation of mass implies that the flux, $\mathbf{J} = c\mathbf{u} - D\nabla c$, must be continuous across Γ, so that

$$(c_t\mathbf{u}_t - D_t\nabla c_t)\cdot\mathbf{n} = (c_c\mathbf{u}_c - D_c\nabla c_c)\cdot\mathbf{n} \quad \text{on } \Gamma. \tag{11}$$

To close the problem, we need one more boundary condition for the species concentration on Γ. The nature of this final boundary condition is not as clear, and we consider three options in this paper. The choice of which boundary condition is appropriate should be motivated by the physiological situation under investigation.

Option 1 (Continuity of Concentration). The simplest boundary condition is to apply continuity of species concentration,

$$c_c = c_t \quad \text{on } \Gamma. \tag{12}$$

Option 2 (A Concentration Jump Proportional to **J** (Membrane Law)). A second option is to use a membrane treatment that links the flux of a species across the interface to the concentration jump across it through the permeability r (r has units $\mathrm{cm\,s^{-1}}$). This approach is used widely in the literature (Jain, 1987, 1990) and stipulates that, in dimensional form,

$$(c_c\mathbf{u}_c - D_c\nabla c_c)\cdot\mathbf{n} = (c_t\mathbf{u}_t - D_r\nabla c_t)\cdot\mathbf{n} = r(c_c - c_t) \quad \text{on } \Gamma. \tag{13}$$

Option 3 (A Concentration Jump as a Consequence of Species Solubility). The final option is a jump in the species concentrations across the interface Γ as a consequence of reduced agent solvability in the interstitium compared to the blood (for gases, this is Henry's law; the concentration and partial pressure of a gas in solution are related through $c = \gamma p$ where γ is the solvability). In this case,

$$\beta c_c = c_t \quad \text{on } \Gamma, \tag{14}$$

for some constant β.

Before we can perform any systematic asymptotic analysis, we must first non-dimensionalize the equations.

2.3. Non-dimensionalization

We non-dimensionalize the model to reduce the number of parameters and to enable us to estimate the relative importance of the various terms. We set

$$\mathbf{X} = d\mathbf{X}', \qquad p = \frac{\mu LU}{d^2}p' + p_0, \qquad \mathbf{u} = U\mathbf{u}', \qquad t = \frac{d}{U}t', \qquad c = Cc', \tag{15}$$

where d and L are the micro- and macro-reference length scales, U is a typical velocity, p_0 is a reference pressure, and C is a typical concentration. We apply these scalings to the fluid and drug transport problems in turn, and from this point onwards drop the prime notation. For ease of the reader, we restate the definition of ε, the ratio of micro- to macro-length scales

$$\varepsilon = \frac{d}{L} \ll 1. \tag{16}$$

2.3.1. Fluid transport
The dimensionless fluid problem is given by

$$\nabla \cdot \mathbf{u}_t = 0 \quad \text{in } \Omega_t, \tag{17}$$

$$\mathbf{u}_t = -\kappa \nabla p_t \quad \text{in } \Omega_t, \tag{18}$$

$$\nabla \cdot \mathbf{u_c} = 0 \quad \text{in } \Omega_c, \tag{19}$$

$$\varepsilon \,\mathrm{Re}\left(\frac{\partial \mathbf{u}_c}{\partial t} + (\mathbf{u}_c \cdot \nabla)\mathbf{u}_c \right) = -\nabla p_c + \varepsilon \nabla^2 \mathbf{u}_c \quad \text{in } \Omega_c, \tag{20}$$

$$\mathbf{u}_c \cdot \mathbf{n} = \mathbf{u}_t \cdot \mathbf{n} = R(p_c - p_t) \quad \text{on } \Gamma, \tag{21}$$

$$\big[(\mathbf{n} \cdot \nabla)\mathbf{u}_c\big] \cdot \boldsymbol{\tau} = -\phi \mathbf{u}_c \cdot \boldsymbol{\tau} \quad \text{on } \Gamma, \tag{22}$$

where

$$\mathrm{Re} = \frac{\rho U d}{\mu}, \qquad \kappa = \frac{kL}{d^3}, \qquad R = \frac{\mu L_p L}{d^2}, \qquad \phi = \frac{\alpha d}{\sqrt{k}}, \tag{23}$$

are dimensionless parameters. In Ω_t, it is possible to eliminate the fluid velocity, $\mathbf{u}_t$, and express the problem in terms of the pressures only as

$$\nabla^2 p_t = 0 \quad \text{in } \Omega_t, \tag{24}$$

$$-\nabla p_t \cdot \mathbf{n} = \psi(p_c - p_t) \quad \text{on } \Gamma. \tag{25}$$

The parameter $\psi = R/\kappa$ is a measure of the permeability of the vascular wall relative to that of the interstitium. It is this ratio that determines the level of fluid leakage out of the capillaries into the interstitium.

2.3.2. Drug transport problem
We define the local Péclet number, Pe_l, as the dimensionless parameter representing the ratio of diffusive to convective timescales on the local length scale,

$$\mathrm{Pe}_l = \frac{U d}{D_c}. \tag{26}$$

Similarly, we define the Damköhler number, Da, as the dimensionless parameter representing the ratio of convective to reactive timescales in the interstitium,

$$\mathrm{Da} = \frac{\lambda d}{U}. \tag{27}$$

The dimensionless drug transport problem is given by

$$\frac{\partial c}{\partial t} + \nabla \cdot (c\mathbf{u} - A\nabla c) = -\mathcal{R}c \quad \text{in } \Omega, \tag{28}$$

where $A_c = 1/\mathrm{Pe}_l$ and $A_t = D_t/(D_c\,\mathrm{Pe}_l)$, and

$$\mathcal{R} = \begin{cases} 0 & \text{in } \Omega_c, \\ \mathrm{Da} & \text{in } \Omega_t. \end{cases} \tag{29}$$

The flux boundary condition (11) is given in dimensionless form by

$$(c_t\mathbf{u}_t - A_t\nabla c_t)\cdot\mathbf{n} = (c_c\mathbf{u}_c - A_c\nabla c_c)\cdot\mathbf{n} \quad \text{on } \Gamma, \tag{30}$$

whereas the Dirichlet boundary conditions (12), (14) remain unchanged. The membrane treatment boundary condition (13) becomes

$$(c_c\mathbf{u}_c - A_c\nabla c_c)\cdot\mathbf{n} = (c_t\mathbf{u}_t - A_t\nabla c_t)\cdot\mathbf{n} = \Upsilon(c_c - c_t) \quad \text{on } \Gamma, \tag{31}$$

where $\Upsilon = r/U$ is a dimensionless parameter.

2.4. Parameter values

Parameter ranges pertaining to the fluid transport problem are discussed in detail (Chapman et al., 2008). Here, we present briefly some of the reported values of the geometrical and physiological parameters and discuss the implications for the nondimensional parameters that characterize the fluid and drug transport problems.

2.4.1. Geometrical parameters

Geometrical data on capillaries are presented in Chapman et al. (2008). A representative mean intercapillary distance d is 50 μm (Less et al., 1991), and the typical size of a vascular tumour $L \approx 1$–10 cm (Kirkpatrick et al., 2003). This gives values of ε between 5×10^{-4} and 5×10^{-3}, justifying the assumption $\varepsilon \ll 1$.

2.4.2. Fluid physiological parameters

Values of the hydraulic conductivity $\kappa = k/\mu$ for different tissues are summarized in Chapman et al. (2008) and lie in the range 10^{-9} to 10^{-6} $\mathrm{cm^3\,s\,kg^{-1}}$. The blood viscosity, μ, depends on the hematocrit (the density of red blood cells) and the temperature, and (though we are approximating blood as a Newtonian fluid) also on the shear rate. Nevertheless, for a normal 40% hematocrit and 37°C, $\mu \approx 4 \times 10^{-3}$ $\mathrm{kg\,m^{-1}\,s^{-1}}$ (Rand et al., 1964). On this basis, the interstitial permeability k lies between 4×10^{-14} and 4×10^{-11} $\mathrm{cm^2}$.

Values of the vascular hydraulic permeability L_p for tumours are summarized in Chapman et al. (2008) and are about 10^{-6} $\mathrm{cm^2\,s\,kg^{-1}}$. The final parameters needed to determine the non-dimensional parameters Re, κ and R are the blood density, ρ, and the typical capillary blood velocity, U. These are $\rho \approx 1040$ $\mathrm{kg\,m^{-3}}$ (Kenner, 1989) and $U \approx 200$ $\mathrm{\mu m\,s^{-1}}$ (Intaglietta et al., 1975).

Based on these values, the Reynolds number $\mathrm{Re} \approx 2.6 \times 10^{-3} = \mathcal{O}(\varepsilon)$ and, therefore, inertia is unimportant on the micro-scale at leading order. We write $\mathrm{Re} = \varepsilon\,\mathrm{Re}_g$ where

Table 1 Data on the diffusion coefficients and uptake rates of a variety of anti-cancer agents

Agent	Blood Diffusion Coefficient, D_c ($cm^2\,s^{-1}$)	Tissue Diffusion Coefficient, D_t ($cm^2\,s^{-1}$)	Tissue Uptake Rate, λ (min^{-1})	Reference
[^{14}C]-sucrose	7.0×10^{-6}	$4.2 \pm 0.9 \times 10^{-8}$	0	Modok et al. (2006)
[^{3}H]-vinblastine	3.3×10^{-6}	$1.9 \pm 0.2 \times 10^{-8}$	6.42×10^{-10}	Yao et al. (2000), Modok et al. (2006)
[^{14}C]-Pt(II)	8.2×10^{-6}	$17.5 \pm 2.6 \times 10^{-8}$	$17.7 \pm 5.5 \times 10^{-2}$	Modok et al. (2007)
[^{14}C]-Pt(IV)	8.2×10^{-6}	$17.8 \pm 3.1 \times 10^{-8}$	$16.2 \pm 5.3 \times 10^{-2}$	Modok et al. (2007)
Tirapazamine (TPZ)	/	$0.40 \pm 0.02 \times 10^{-6}$	1.12 ± 0.08	Hicks et al. (2006)
TPZ Analogue 3	/	$0.027 \pm 0.015 \times 10^{-6}$	19.90 ± 6.61	Hicks et al. (2006)
TPZ Analogue 10	/	$1.87 \pm 0.17 \times 10^{-6}$	3.68 ± 0.39	Hicks et al. (2006)
TPZ (V79-171b MCLs) oxic	8.8×10^{-6}	$7.4 \pm 0.3 \times 10^{-7}$	0	Hicks et al. (1998)
TPZ (V79-171b MCLs) anoxic	8.8×10^{-6}	$7.4 \pm 0.3 \times 10^{-7}$	0.52 ± 0.08	Hicks et al. (1998)
TPZ (MGH-U1 MCLs) oxic	1.5×10^{-5}	$1.25 \pm 0.16 \times 10^{-6}$	0	Hicks et al. (1998)
TPZ (MGH-U1 MCLs) anoxic	1.5×10^{-5}	$1.25 \pm 0.16 \times 10^{-6}$	0.31 ± 0.03	Hicks et al. (1998)

$\mathrm{Re}_g = \rho U L/\mu$ represents the Reynolds number on the global length scale, and is $\mathcal{O}(1)$. Also, R lies in the range 1.6×10^{-6} to 1.6×10^{-5} and κ in the range 3.2×10^{-5} to 3.2×10^{-3}. The limit we consider is $\varepsilon \to 0$ with $R/\varepsilon = \bar{R}$ and $\varepsilon\kappa = \bar{\kappa}$ fixed (the permeability ratio ψ is thus of order ε^2, and we define $\psi/\varepsilon^2 = \bar{\psi}$ where $\bar{\psi}$ is fixed as $\varepsilon \to 0$). This is a distinguished limit, in that it retains the greatest number of physical phenomena at leading order. Thus, although κ may be smaller, it is quite sensitive to the choice of d, and it is important to retain it in the asymptotic analysis.

The limit $\varepsilon \to 0$ with $\bar{\kappa} = k/d^2$ fixed corresponds to the case when $\phi = \mathcal{O}(\alpha)$. As far as we know, there is no physiological data available for α. We therefore assume $\phi = \mathcal{O}(1)$, which again represents a distinguished limit.

In conclusion, we consider the limit $\varepsilon \to 0$ keeping the dimensionless fluid parameters

$$\mathrm{Re}_g = \rho U L/\mu, \quad \bar{\kappa} = k/d^2, \quad \bar{R} = \mu L_p L^2/d^3, \quad \bar{\psi} = \mu L_p L^2/kd, \quad \phi = \alpha d/\sqrt{k}, \tag{32}$$

fixed.

2.4.3. Drug physiological parameters

Despite the fundamental important of drug transport in predicting drug distribution in tumours, it is rare that the transport properties of anticancer agents are fully characterized. Therefore, vital information about the relative contributions of diffusivity, convection, cellular uptake, and metabolism to intra-tumoural drug kinetics is often missing. Two research groups have addressed this and have focussed on measuring the diffusion coefficients and uptake rates of various drugs in multicell layer (MCL) experiments. This

experimental setup does not include flow, and so provides a simplified in vitro environment in which to accurately measure these quantities; their findings are presented in Table 1. Modok and co-authors measured the transport properties of [^{14}C]-sucrose, [^{3}H]-vinblastine, [^{14}C]-Pt(II), and [^{14}C]-Pt(IV) in their papers (Modok et al., 2006, 2007) using MCL tumour models comprising DLD1 colon cancer cells. [^{14}C]-sucrose is a commonly used tracer molecule (i.e. does not react in the interstitium), [^{3}H]-vinblastine is a cell cycle-specific anticancer drug used widely in cancer therapies, and four-coordinate platinum-based anticancer drugs are widely used in primary or palliative chemotherapy (in particular for testicular cancer). In contrast, Hicks and co-authors measured the drug transport properties for Tirapazamine (TPZ) (and various analogues of TPZ) in oxic and anoxic conditions in their papers (Hicks et al., 1998, 2006). TPZ is a hypoxia-selective cytotoxic agent, designed to target the hypoxic regions of tumours which may be left un-reached by most standard intravenous therapies. Next we discuss the dimensionless parameters for the drug transport problem in turn.

The Péclet number The local Péclet number, Pe_l, is calculated based on the diffusion coefficient in the blood for each agent in Table 2. Maximum and minimum values are presented, based on the maximum and minimum values of the local length scale d. The appropriate scaling as $\varepsilon \to 0$ is that $\mathrm{Pe}_l = \mathcal{O}(1)$. The local Péclet number, Pe_l is related to the global Péclet number, $\mathrm{Pe}_g = UL/D_c$, through the scaling

$$\mathrm{Pe}_g = \frac{1}{\varepsilon}\mathrm{Pe}_l. \tag{33}$$

This global Péclet number, Pe_g represents the ratio of diffusive to advective time scales on the global length scale. Thus whilst advection and diffusion balance in the capillaries on the local length scale, advection dominates over diffusion on the global length scale.

The dimensionless diffusivity in the interstitium The dimensionless diffusivity in the interstitium represents the ratio of dimensional diffusivities $D_r = D_t/D_c$, and the possible values for this ratio are presented in Table 2. For these data, $D_r = \mathcal{O}(\varepsilon)$ and so there is a jump in the value of the diffusion coefficient across the blood-interstitium membrane Γ. In this case, we assume that the fluid velocity in the tissue is also $\mathcal{O}(\varepsilon)$, as it is unlikely that advection dominates in the tissue on the micro-scale. However, these agents only represent a small proportion of those available, and so we consider both this case and that when $D_r = \mathcal{O}(1)$, in which the agent diffusivities are the same order of magnitude in both the blood and tissue.

The Damköhler number Maximum and minimum values for the Damköhler number, Da are presented in Table 2. Clearly, for the tracer molecules ([^{14}C]-sucrose, and TPZ (V79-171b MCLs), TPZ (MGH-U1 MCLs) in oxic conditions) $\mathrm{Da} = 0$ as there is no uptake in the interstitium. The Damköhler number for [^{3}H]-vinblastine is insignificant, and so [^{3}H]-vinblastine should also be treated as a tracer molecule. For the remaining agents, $\mathrm{Da} = \mathcal{O}(\varepsilon)$. However, the agents presented here only reflect a small proportional of those used in practice. To cover all options, we consider $\mathrm{Da} = \mathcal{O}(1)$ to be the maximum feasible value for the Damköhler number, and so retain all transport features at leading-order. In this way, it remains possible to take limiting cases to test smaller values of Da.

Table 2 The dimensionless parameters Pe_l (calculated using D_c), Da, and D_r for a variety of anti-cancer agents. The velocity scale is $U = 0.02\ \mathrm{cm\,s^{-1}}$, and the maximum/minimum values presented are based on the range of values for the length scale d

Agent	Pe_l Range	D_r	Da Range
[^{14}C]-sucrose	51.7 to 16.1	6.0×10^{-3}	0
[^{3}H]-vinblastine	109.8 to 29.7	5.8×10^{-3}	5.81×10^{-10} to 1.57×10^{-10}
[^{14}C]-Pt(II)	44.2 to 12.0	2.1×10^{-2}	2.67×10^{-3} to 7.23×10^{-4}
[^{14}C]-Pt(IV)	45.3 to 12.0	2.1×10^{-2}	2.44×10^{-3} to 6.62×10^{-4}
Tirapazamine (TPZ)	/	/	1.69×10^{-2} to 4.57×10^{-3}
TPZ Analogue 3	/	/	0.300 to 8.12×10^{-2}
TPZ Analogue 10	/	/	5.55×10^{-2} to 1.50×10^{-2}
TPZ (V79-171b MCLs) oxic	41.2 to 11.1	8.4×10^{-2}	0
TPZ (V79-171b MCLs) anoxic	41.2 to 11.1	8.4×10^{-2}	7.85×10^{-3} to 2.12×10^{-3}
TPZ (MGH-U1 MCLs) oxic	24.1 to 6.53	8.3×10^{-2}	0
TPZ (MGH-U1 MCLs) anoxic	24.1 to 6.53	8.3×10^{-2}	4.67×10^{-3} to 1.27×10^{-3}

Table 3 Calculations of the dimensionless parameter $\Upsilon = r/U$ based on MCL experiments by Modok and co-authors. In each case, $U = 0.02\ \mathrm{cm\,s^{-1}}$ is used and the appropriate scaling is $\Upsilon = \mathcal{O}(\varepsilon)$

Agent	r ($\mathrm{cm\,s^{-1}}$)	Υ	Reference
[^{14}C]-sucrose	$1.4 \pm 0.3 \times 10^{-4}$	0.7×10^{-2}	Modok et al. (2006)
[^{3}H]-vinblastine	$1.2 \pm 0.2 \times 10^{-4}$	0.6×10^{-2}	Modok et al. (2006)
[^{14}C]-Pt(II)	$2.7 \pm 0.6 \times 10^{-5}$	1.35×10^{-3}	Modok et al. (2007)
[^{14}C]-Pt(IV)	$2.5 \pm 0.4 \times 10^{-5}$	1.25×10^{-3}	Modok et al. (2007)

The membrane coefficient To the best of our knowledge, r has not been measured in vivo; Modok and co-authors determined r for their MCL experiments in Modok et al. (2006, 2007), and although they are calculated for a different membrane they serve to give an order of magnitude estimate. Values for r and the corresponding dimensionless parameter Υ are shown in Table 3 for the four anti-cancer agents tested by Modok et al. These values indicate that the appropriate scaling is $\Upsilon = \mathcal{O}(\varepsilon)$ and so we define $\bar{\Upsilon}$ through $\Upsilon = \varepsilon\bar{\Upsilon}$ where $\bar{\Upsilon} = \mathcal{O}(1)$.

The solubility ratio To the best of our knowledge, there is no data available for β. We determine the appropriate scaling for β with ε as part of the analysis that follows.

3. Multiple-scales analysis

We use the method of multiple-scales to move from the local to the global description and derive continuum equations describing fluid and drug transport on the macro-scale. A similar approach is used for fluid transport in fractured rock systems in Arbogast et al. (1990, 1991), Arbogast and Lehr (2006) and resulted in a similar dual-porosity model on the macro-scale.

As $\varepsilon \ll 1$, the micro- and macro-length scales are well separated and we define the variables representing them as $\mathbf{X}$ and $\mathbf{x} = \varepsilon\mathbf{X}$, respectively. Currently, we are on the

timescale for advection on the micro-scale (which is d/U); however, we seek the macroscopic behaviour and, therefore, must move onto the timescale for advection on the macroscale (which is L/U). This is achieved by rescaling

$$t = \frac{t}{\varepsilon}, \tag{34}$$

which we refer to as the 'advective rescaling'. Under the assumption of scale separation, $\mathbf{X}$ and $\mathbf{x}$ can be treated as independent variables, so that

$$\boldsymbol{\nabla} = \boldsymbol{\nabla}_X + \varepsilon \boldsymbol{\nabla}_x, \qquad \nabla^2 = \nabla_X^2 + 2\varepsilon \boldsymbol{\nabla}_x \cdot \boldsymbol{\nabla}_X + \varepsilon^2 \nabla_x^2. \tag{35}$$

Henceforth, we denote the vasculature–interstitium interface by Γ_ϵ to emphasise its dependence on the micro-scale variable, and define averages over the interstitial, capillary and entire micro-scale domains by

$$\langle s \rangle_t = \frac{1}{|\Omega_t|} \int_{\Omega_t} s \, \mathrm{d}V, \qquad \langle s \rangle_c = \frac{1}{|\Omega_c|} \int_{\Omega_c} s \, \mathrm{d}V, \qquad \langle s \rangle = \frac{1}{|\Omega|} \int_{\Omega} s \, \mathrm{d}V, \tag{36}$$

and the capillary volume fraction, and its complement, by

$$n_c = \frac{|\Omega_c|}{|\Omega|}, \qquad n_t = \frac{|\Omega_t|}{|\Omega|} = 1 - n_c. \tag{37}$$

We consider the fluid and drug transport problems in turn.

3.1. Fluid problem

The fluid transport equations in Ω are now given by

$$\nabla_X^2 p_t + 2\varepsilon \boldsymbol{\nabla}_x \cdot \boldsymbol{\nabla}_X p_t + \varepsilon^2 \nabla_x^2 p_t = 0 \quad \text{in } \Omega_t, \tag{38}$$

$$\varepsilon \mathbf{u}_t = -\bar{\kappa} \boldsymbol{\nabla}_X p_t - \varepsilon \bar{\kappa} \boldsymbol{\nabla}_x p_t \quad \text{in } \Omega_t, \tag{39}$$

$$\boldsymbol{\nabla}_X \cdot \mathbf{u}_c + \varepsilon \boldsymbol{\nabla}_x \cdot \mathbf{u}_c = 0 \quad \text{in } \Omega_c, \tag{40}$$

$$\varepsilon^2 \mathrm{Re}_g \left(\varepsilon \frac{\partial \mathbf{u}_c}{\partial t} + (\mathbf{u}_c \cdot \boldsymbol{\nabla}_X)\mathbf{u}_c + \varepsilon (\mathbf{u}_c \cdot \boldsymbol{\nabla}_x)\mathbf{u}_c \right) = -\boldsymbol{\nabla}_X p_c - \varepsilon \boldsymbol{\nabla}_x p_c + \varepsilon \nabla_X^2 \mathbf{u}_c + 2\varepsilon^2 \boldsymbol{\nabla}_X \cdot \boldsymbol{\nabla}_x \mathbf{u}_c + \varepsilon^3 \nabla_x^2 \mathbf{u}_c \quad \text{in } \Omega_c, \tag{41}$$

$$-\boldsymbol{\nabla}_X p_t \cdot \mathbf{n} - \varepsilon \boldsymbol{\nabla}_x p_t \cdot \mathbf{n} = \varepsilon^2 \bar{\psi} (p_c - p_t) \quad \text{on } \Gamma_\epsilon, \tag{42}$$

$$\mathbf{u}_c \cdot \mathbf{n} = \varepsilon \bar{R} (p_c - p_t) \quad \text{on } \Gamma_\epsilon, \tag{43}$$

$$\big[(\mathbf{n} \cdot \boldsymbol{\nabla}_X)\mathbf{u}_c\big] \cdot \boldsymbol{\tau} + \varepsilon \big[(\mathbf{n} \cdot \boldsymbol{\nabla}_x)\mathbf{u}_c\big] \cdot \boldsymbol{\tau} = -\phi \mathbf{u}_c \cdot \boldsymbol{\tau} \quad \text{on } \Gamma_\epsilon. \tag{44}$$

We perform a multiple-scales expansion

$$\mathbf{u} = \mathbf{u}^{(0)}(\mathbf{x}, \mathbf{X}) + \varepsilon \mathbf{u}^{(1)}(\mathbf{x}, \mathbf{X}) + \cdots, \tag{45}$$

$$p = p^{(0)}(\mathbf{x}, \mathbf{X}) + \varepsilon p^{(1)}(\mathbf{x}, \mathbf{X}) + \cdots, \tag{46}$$

where we require that all variables are periodic in $\mathbf{X}$.

3.1.1. Interstitial domain

The equations determining the fluid transport in Ω_t are (38), (39), and (42). Equating coefficients of ε^0 in (38) and (42) yields

$$\nabla_X^2 p_t^{(0)} = 0 \quad \text{in } \Omega_t \text{ with } \nabla_X p_t^{(0)} \cdot \mathbf{n} = 0 \text{ on } \Gamma_\epsilon, \tag{47}$$

with $p_t^{(0)}$ periodic in $\mathbf{X}$. Therefore, $p_t^{(0)}$ must be constant on the local scale, so that $p_t^{(0)} = p_t^{(0)}(\mathbf{x})$. Equating coefficients of ε in (38) and (42) gives

$$\nabla_X^2 p_t^{(1)} = 0 \quad \text{in } \Omega_t \text{ with } \nabla_X p_t^{(1)} \cdot \mathbf{n} = -\nabla_x p_t^{(0)} \cdot \mathbf{n} \text{ on } \Gamma_\epsilon. \tag{48}$$

Unlike $p_t^{(0)}$, $p_t^{(1)}$ is not locally uniform due to the non-homogeneous flux boundary condition on Γ_ϵ. To solve for $p_t^{(1)}$, we exploit the linearity of (48) and propose a solution of the form

$$p_t^{(1)} = -\frac{\partial p_t^{(0)}}{\partial x_j} P_t^j(\mathbf{X}) + \bar{p}_t^{(1)}(\mathbf{x}), \tag{49}$$

where $P_t^j(\mathbf{X})$ and $\bar{p}_t^{(1)}$ are to be determined, and $j = 1, 2, 3$ correspond to the Cartesian coordinate directions (we have used the summation convention). The function $P_t^j(\mathbf{X})$ depends on the local variable only, and accounts for the local variation in the $\mathcal{O}(\varepsilon)$ pressure term $p_t^{(1)}$. It is determined by solving the cell problem

$$\nabla_X^2 P_t^j = 0 \quad \text{in } \Omega_t \text{ with } \mathbf{n} \cdot \nabla_X P_t^j = \mathbf{n} \cdot \mathbf{e}_j \text{on } \Gamma_\epsilon, \tag{50}$$

where $\mathbf{e}_j$ denotes the unit vector in the j-direction, and P_t^j is periodic in $\mathbf{X}$. The variable P_t^j is not determined uniquely by this cell problem, and so we impose the additional condition

$$\left\langle P_t^j \right\rangle_t = 0. \tag{51}$$

Equation (51) ensures uniqueness of the solution, and gives $\langle p_t^{(1)} \rangle_t = \overline{p}_t^{(1)}$. Finally, equating coefficients at $\mathcal{O}(\varepsilon^2)$ gives

$$\nabla_X^2 p_t^{(2)} + 2\nabla_x \cdot \nabla_X p_t^{(1)} + \nabla_x^2 p_t^{(0)} = 0 \quad \text{in } \Omega_t, \tag{52}$$

$$-\nabla_X p_t^{(2)} \cdot \mathbf{n} - \nabla_x p_t^{(1)} \cdot \mathbf{n} = \bar{\psi}\left(p_c^{(0)} - p_t^{(0)}\right) \quad \text{on } \Gamma_\epsilon. \tag{53}$$

Equations (52)–(53) can be used to derive the first continuum pressure equation. First, we integrate (52) over Ω_t, and use the divergence theorem to transform it to an integral over the surfaces bounding Ω_t. These surfaces are comprised of the capillary walls Γ_ϵ, together with sections of the outer surface of the periodic unit cell. The contribution from the unit cell boundaries to the resulting surface integral cancel out due to periodicity. This leaves only the contributions from the capillary surface Γ_ϵ, which are evaluated using the boundary condition (53) to give

$$\bar{\kappa} \nabla_x \cdot \left(\mathbf{E} \cdot \nabla_x p_t^{(0)}\right) = \frac{\bar{R}}{|\Omega|} \int_{\Gamma_\epsilon} \left(p_t^{(0)} - p_c^{(0)}\right) \mathrm{d}S, \tag{54}$$

where

$$\mathrm{E}_{ij} = \delta_{ij} + \frac{1}{|\Omega_t|}\int_{\Gamma_\epsilon} P_t^j n_i \,\mathrm{d}S. \tag{55}$$

Equation (54) is a coupled continuum equation for $p_c^{(0)}$ and $p_t^{(0)}$ on the macro-scale; a second equation will be derived from the fluid system in Ω_c in Section 3.1.2. Finally, equating $\mathcal{O}(\varepsilon)$ terms in the velocity Eq. (39) leaves an expression for the leading-order fluid velocity in the interstitium,

$$\left\langle \mathbf{u}_t^{(0)} \right\rangle_t = -\bar{\kappa}\mathbf{E}\cdot\nabla_x p_t^{(0)}. \tag{56}$$

3.1.2. Capillary domain
Equating powers of ε^0 in (41) yields

$$\nabla_X p_c^{(0)} = 0. \tag{57}$$

Thus, $p_c^{(0)} = p_c^{(0)}(\mathbf{x})$ and the leading-order capillary pressure is constant on the local scale. Equating powers of ε^1 in (41), and ε^0 in (40), (43), and (44) yields

$$\nabla_X p_c^{(1)} - \nabla_X^2 \mathbf{u}_c^{(0)} = -\nabla_x p_c^{(0)} \quad \text{in } \Omega_c, \tag{58}$$

$$\nabla_X \cdot \mathbf{u}_c^{(0)} = 0 \quad \text{in } \Omega_c, \tag{59}$$

$$\mathbf{u}_c^{(0)} \cdot \mathbf{n} = 0 \quad \text{on } \Gamma_\epsilon, \tag{60}$$

$$\left[(\mathbf{n}\cdot\nabla_X)\mathbf{u}_c^{(0)}\right]\cdot\boldsymbol{\tau} = -\phi\mathbf{u}_c^{(0)}\cdot\boldsymbol{\tau} \quad \text{on } \Gamma_\epsilon. \tag{61}$$

We solve for $\mathbf{u}_c^{(0)}$ and $p_c^{(1)}$ by exploiting linearity and proposing solutions of the form

$$\mathbf{u}_c^{(0)} = -\frac{\partial p_c^{(0)}}{\partial x_j}\mathbf{w}_c^j(\mathbf{X}), \tag{62}$$

$$p_c^{(1)} = -P_c^j \frac{\partial p_c^{(0)}}{\partial x_j}(\mathbf{X}) + \bar{p}_c^{(1)}(\mathbf{x}). \tag{63}$$

The cell variables $\mathbf{w}_c^j$ and P_c^j are determined by substituting (62)–(63) into (59), (58), (73), and (61) to give the cell problem

$$\nabla_X \cdot \mathbf{w}_c^j = 0 \quad \text{in } \Omega_c, \tag{64}$$

$$\nabla_X P_c^j = \nabla_X^2 \mathbf{w}_c^j + \mathbf{e}_j \quad \text{in } \Omega_c, \tag{65}$$

$$\mathbf{n}\cdot\mathbf{w}_c^j = 0 \quad \text{on } \Gamma_\epsilon, \tag{66}$$

$$\left[(\mathbf{n}\cdot\nabla_X)\mathbf{w}_c^j\right]\cdot\boldsymbol{\tau} = -\phi\mathbf{w}_c^j\cdot\boldsymbol{\tau} \quad \text{on } \Gamma_\epsilon, \tag{67}$$

with $\mathbf{w}_c^j$ and P_c^j periodic in $\mathbf{X}$. The variable P_c^j is not determined uniquely by this cell problem, and so we impose the additional condition

$$\left\langle P_c^j \right\rangle_c = 0. \tag{68}$$

The canonical cell problem (64)–(67) can be solved numerically for a prescribed vascular configuration. Defining,

$$\mathrm{K}_{ij} = \frac{1}{|\Omega_c|}\int_{\Omega_c} w_{ci}^{j}\,\mathrm{d}V, \tag{69}$$

and integrating (62) gives Darcy's Law for the averaged capillary fluid pressure

$$\left\langle \mathbf{u}_c^{(0)} \right\rangle_c = -\mathbf{K}\cdot\nabla_x p_c^{(0)}. \tag{70}$$

Therefore, it can be seen that the inclusion of the slip boundary condition (8) has a direct impact on the effective permeability of the capillary bed through $\mathbf{K}$. Integrating (63) yields

$$\left\langle p_c^{(1)} \right\rangle_c = \bar{p}_c^{(1)}. \tag{71}$$

Equating coefficients of ε^1 in (40), (43), and (44) gives

$$\nabla_X\cdot\mathbf{u}_c^{(1)} + \nabla_x\cdot\mathbf{u}_c^{(0)} = 0 \quad \text{in } \Omega_c, \tag{72}$$

$$\mathbf{u}_c^{(1)}\cdot\mathbf{n} = \bar{R}\left(p_c^{(0)} - p_t^{(0)}\right) \quad \text{on } \Gamma_\epsilon, \tag{73}$$

$$\left[(\mathbf{n}\cdot\nabla_X)\mathbf{u}_c^{(1)}\right]\cdot\boldsymbol{\tau} + \left[(\mathbf{n}\cdot\nabla_x)\mathbf{u}_c^{(0)}\right]\cdot\boldsymbol{\tau} = -\phi\mathbf{u}_c^{(1)}\cdot\boldsymbol{\tau} \quad \text{on } \Gamma_\epsilon. \tag{74}$$

Equations (72) and (73) can be used to derive the second continuum pressure equation. Integrating (72) over the fluid domain, using the divergence theorem to transform this to a surface integral, and finally using periodicity with (73) gives the second homogenized equation for $p_c^{(0)}$ and $p_t^{(0)}$, namely

$$\nabla_x\cdot\left(\mathbf{K}\cdot\nabla_x p_c^{(0)}\right) = \frac{\bar{R}S}{|\Omega_c|}\left(p_c^{(0)} - p_t^{(0)}\right), \tag{75}$$

where S is the total capillary surface area in the unit cell, defined by

$$S = \int_{\Gamma_\epsilon}\mathrm{d}S. \tag{76}$$

Equation (75) should be solved in conjunction with (54) on the global domain, subject to appropriate boundary conditions. The final continuum model that we have arrived at is that of a double porous medium (for the vasculature and interstitium), with transport between them due to the higher vascular permeability in tumours. This extends the result of Chapman et al. (2008) to account for an arbitrary periodic micro-scale geometry, and the slip boundary condition for a Newtonian fluid flowing over a permeable boundary. It can be shown that, in the limit when the capillaries are thin, and the capillary grid takes a grid geometry, the effective permeabilities reduce to those derived in Chapman et al. (2008).

It is now possible to test the impact that vascular structure has on tumour-scale fluid perfusion. First of all, the fluid permeability tensors $\mathbf{E}$ and $\mathbf{K}$ must be determined for different vascular structures (e.g. a regular honeycomb pattern that may represent the microcirculation in healthy tissue, and more irregular structures to mimic those found

in different tumour types in Konerding et al. (1999, 2001)). This will be achieved by solving the cell problems (50) and (64)–(67) on the appropriate micro-scale structures. Equations (54) and (75) for the interstitial and capillary pressures can then be solved on an appropriate global domain (extracted, for example, from a tumour image), with Dirichlet boundary conditions on the capillary pressure, p_c, to simulate a pressure drop across the capillary bed. It is anticipated that variations in underlying vascular structure will result in different interstitial and capillary fluid pressure distributions, as a direct consequence of the change in the tensors $\mathbf{E}$ and $\mathbf{K}$.

3.2. Drug problem

Next, we consider the drug transport problem. It is beyond the scope of this paper to present the results of every feasible scaling of Da and D_r, together with each of the three possible boundary conditions mentioned. Therefore, we consider five key examples, and note that most remaining options can be determined as limiting cases of these examples:

1. *Tracer Transport*: we consider the simplest example in which there is no reaction (so that $\mathrm{Da} = 0$), $D_r = \mathcal{O}(1)$ and there is continuity of tracer concentration and flux on Γ_ϵ.
2. *Strong Reaction:* $\mathrm{Da} = \mathcal{O}(1)$. In this case, if the concentration is continuous across Γ_ϵ then the consumption in the interstitium will exhaust the supply over the microscopic length scale ε. The only way to propagate c over large distances is if the solubility in the interstitium is much less than that in blood so that boundary condition (14) is used with $\beta = \mathcal{O}(\varepsilon)$. Therefore, we consider the case when $\mathrm{Da} = \mathcal{O}(1)$ and $D_r = \mathcal{O}(1)$ together with the concentration jump boundary condition (14).
3. *Weak Reaction, Large Interstitial Diffusion:* $\mathrm{Da} = \mathcal{O}(\varepsilon)$ and $D_r = \mathcal{O}(1)$, with continuity of concentration and flux on Γ.
4. *Weak Reaction, Large Interstitial Diffusion:* $\mathrm{Da} = \mathcal{O}(\varepsilon)$ and $D_r = \mathcal{O}(1)$, with the membrane law boundary condition (31).
5. *Weak Reaction, Small Interstitial Diffusion:* $\mathrm{Da} = \mathcal{O}(\varepsilon)$ and $D_r = \mathcal{O}(\varepsilon)$ with the membrane law boundary condition (31).

For each of the five options detailed above, we apply the same asymptotic homogenization strategy. Given the advective rescaling (34) and assumption of scale separation (35), the species transport equations are given by

$$\varepsilon\frac{\partial c}{\partial t}+\varepsilon\nabla_x\cdot(c\mathbf{u})+\nabla_X\cdot(c\mathbf{u})=A\nabla_X^2 c+2A\varepsilon\nabla_x\cdot\nabla_X c+\varepsilon^2 A\nabla_x^2 c-\mathcal{R}c \quad \text{in } \Omega. \tag{77}$$

In addition to (45) and (46), we expand

$$c=c^{(0)}(\mathbf{x},\mathbf{X},t)+\varepsilon c^{(1)}(\mathbf{x},\mathbf{X},t)+\cdots, \tag{78}$$

where all variables are assumed periodic in $\mathbf{X}$; the velocity terms in (77) are already known from the fluid analysis in Section 3.1. We equate powers of ε, considering the $\mathcal{O}(1)$, and $\mathcal{O}(\varepsilon)$ systems in turn. In each case, the $\mathcal{O}(1)$ system determines the form of the leading-order solution $c^{(0)}$. We evaluate the appropriate form of the solvability condition for the $\mathcal{O}(\varepsilon)$ system, and use this to determine the leading-order homogenized transport equation. This will be an advection–reaction equation for the average species concentrations. By examining the solvability condition at $\mathcal{O}(\varepsilon^2)$ it is also possible to determine the $\mathcal{O}(\varepsilon)$

correction to the macro-scale equations derived here; in particular this will bring in the influence of diffusion, although is outside the scope of this paper (further details are given in Shipley, 2008).

3.2.1. Tracer transport

The tracer transport equation is given by (77) with $\mathcal{R} = 0$ throughout Ω. We employ continuity of concentration and flux boundary conditions on Γ_ϵ, which reduce to

$$c_c = c_t, \tag{79}$$

$$(A_c \nabla_X c_c + \varepsilon A_c \nabla_x c_c) \cdot \mathbf{n} = (A_t \nabla_X c_t + \varepsilon A_t \nabla_x c_t) \cdot \mathbf{n}. \tag{80}$$

For ease of notation we define the operator (and its corresponding adjoint)

$$\mathcal{L}_0 \star := A \nabla_X^2 \star - \nabla_X \cdot \left(\mathbf{u}^{(0)} \star\right), \tag{81}$$

$$\mathcal{L}_0^* \star := A \nabla_X^2 \star + \nabla_X \cdot \left(\mathbf{u}^{(0)} \star\right), \tag{82}$$

both equipped with periodic boundary conditions on Ω. Equating coefficients of ε^0 in (77), (79), and (80) gives

$$\mathcal{L}_0 c^{(0)} = 0, \tag{83}$$

subject to boundary conditions

$$c_c^{(0)} = c_t^{(0)} \quad \text{and} \quad A_c \nabla_X c_c^{(0)} \cdot \mathbf{n} = A_t \nabla_X c_t^{(0)} \cdot \mathbf{n} \quad \text{on } \Gamma_\epsilon. \tag{84}$$

This system only has the locally uniform solutions $c^{(0)} = \overline{c}(\mathbf{x}, t)$ everywhere in Ω. Equating coefficients of ε^1 gives

$$\mathcal{L}_0 c^{(1)} = \frac{\partial \overline{c}}{\partial t} + \left(\mathbf{u}^{(0)} \cdot \nabla_x\right) \overline{c} \quad \text{in } \Omega, \tag{85}$$

subject to the internal boundary conditions

$$c_c^{(1)} = c_t^{(1)} \quad \text{and} \quad \left(A_c \nabla_X c_c^{(1)} - A_t \nabla_X c_t^{(1)}\right) \cdot \mathbf{n} = (A_t - A_c) \nabla_x \overline{c} \cdot \mathbf{n} \quad \text{on } \Gamma_\epsilon, \tag{86}$$

where we have used the fact that $c^{(0)} = \overline{c}(\mathbf{x}, t)$ and $\nabla_X \cdot \mathbf{u}^{(1)} = -\nabla_x \cdot \mathbf{u}^{(0)}$. First we determine the appropriate solvability condition for this system according to the Fredholm alternative. We define the stationary invariant distribution $\rho(\mathbf{x}, \mathbf{X})$ as that which solves the homogeneous adjoint problem

$$\mathcal{L}_0^* \rho = 0, \tag{87}$$

with

$$\rho_c = \rho_t \quad \text{and} \quad A_c \nabla_X \rho_c \cdot \mathbf{n} = A_t \nabla_X \rho_t \cdot \mathbf{n} \quad \text{on } \Gamma_\epsilon, \tag{88}$$

and periodic boundary conditions on the periodic cell, where $\rho_t = \rho|_{\Omega_t}$ and $\rho_c = \rho|_{\Omega_c}$. The solution to (87)–(88) is only unique up to normalization, and so we impose the

uniqueness condition

$$\int_V \rho(\mathbf{x}, \mathbf{X})\, \mathrm{d}V = 1. \tag{89}$$

The system (87)–(89) only has the locally uniform solution $\rho = \overline{\rho}(\mathbf{x})$ throughout Ω; the normalization condition (89) determines that $\overline{\rho} = 1/|\Omega|$.

The solvability condition for (85)–(86) is given by

$$\int_\Omega \left(\frac{\partial \overline{c}}{\partial t} + \left(\mathbf{u}^{(0)} \cdot \nabla_x\right)\overline{c} \right) \rho \, \mathrm{d}V = \int_\Omega \left(\rho \mathcal{L}_0 c^{(1)} - c^{(1)} \mathcal{L}_0^* \rho \right) \mathrm{d}V$$
$$= (A_t - A_c) \int\!\!\int_{\Gamma_\epsilon} \rho \nabla_x \overline{c} \cdot \mathbf{n} \, \mathrm{d}S. \tag{90}$$

However, both ρ and $\nabla_x \overline{c}$ are locally uniform, and so this final integral is zero. Therefore, the solvability condition given by (90) reduces to

$$\frac{\partial \overline{c}}{\partial t} + \tilde{\mathbf{u}}^{(0)} \cdot \nabla_x \overline{c} = 0, \tag{91}$$

where $\tilde{\mathbf{u}}^{(0)}$ is the averaged leading-order fluid velocity

$$\tilde{\mathbf{u}}^{(0)} = n_t \left\langle \mathbf{u}_t^{(0)} \right\rangle_t + n_c \left\langle \mathbf{u}_c^{(0)} \right\rangle_c. \tag{92}$$

However, from Eqs. (54), (56), and (70), (75) for the interstitial and capillary fluid pressures and velocities we have that

$$n_c \nabla_x \cdot \left\langle \mathbf{u}_c^{(0)} \right\rangle_c = \frac{\overline{R}S}{|\Omega|} \left(p_t^{(0)} - p_c^{(0)} \right), \qquad n_t \nabla_x \cdot \left\langle \mathbf{u}_t^{(0)} \right\rangle_t = \frac{\overline{R}S}{|\Omega|} \left(p_c^{(0)} - p_t^{(0)} \right). \tag{93}$$

Therefore, $\nabla_x \cdot \tilde{\mathbf{u}}^{(0)} = 0$ and Eq. (91) can also be written in conservation form as

$$\frac{\partial \overline{c}}{\partial t} + \nabla_x \cdot \left(\overline{c} \tilde{\mathbf{u}}^{(0)} \right) = 0. \tag{94}$$

Note that $\langle c \rangle = n_c \langle c_c \rangle_c + n_t \langle c_t \rangle_t = \overline{c}$ is (to leading order) the average tracer concentration. Equation (94) is the leading-order homogenized species transport equation and shows that the average species concentration is simply advected with the combined average fluid velocity $\tilde{\mathbf{u}}^{(0)}$ at leading-order.

3.2.2. Strong reaction with a concentration jump on Γ_ϵ

Next, we consider the case when $\mathrm{Da} = \mathcal{O}(1)$, together with $D_r = \mathcal{O}(1)$ and the concentration jump boundary condition (14). We let $\beta = \varepsilon \overline{\beta}$ with $\overline{\beta}$ of order one, so that

$$\varepsilon \frac{\partial c}{\partial t} + \varepsilon \nabla_x \cdot (c\mathbf{u}) + \nabla_X \cdot (c\mathbf{u}) = A \nabla_X^2 c + 2A\varepsilon \nabla_x \cdot \nabla_X c + \varepsilon^2 A \nabla_x^2 c - \mathcal{R}c \quad \text{in } \Omega, \tag{95}$$

with boundary conditions

$$\varepsilon \overline{\beta} c_c = c_t \quad \text{on } \Gamma_\epsilon, \tag{96}$$

$$(c_c\mathbf{u}_c - A_c\nabla_X c_c - A_c\nabla_x c_c)\cdot\mathbf{n} = (c_t\mathbf{u}_t - A_t\nabla_X c_t - A_t c_t\nabla_x c_t)\cdot\mathbf{n} \quad \text{on } \Gamma_\epsilon. \tag{97}$$

In this case, c_t will be $\mathcal{O}(\varepsilon)$ throughout Ω_t, and so we employ multiple-scales expansions of the form

$$c_c = c_c^{(0)}(\mathbf{x},\mathbf{X},t) + \varepsilon c_c^{(1)}(\mathbf{x},\mathbf{X},t) + \cdots, \tag{98}$$

$$c_t = \varepsilon c_t^{(0)}(\mathbf{x},\mathbf{X},t) + \varepsilon^2 c_t^{(1)}(\mathbf{x},\mathbf{X},t) + \cdots. \tag{99}$$

For ease of notation, we define the operator

$$\mathcal{L}_1\star := A\nabla_X^2\star - \nabla_X\cdot\left(\mathbf{u}^{(0)}\star\right) - \mathcal{R}\star \quad \text{in } \Omega, \tag{100}$$

equipped with periodic boundary conditions on Ω. We perform multiple scales expansions (98)–(99) and equate powers of ε; the systems in Ω_c and Ω_t now decouple so there is no need to introduce an invariant distribution ρ, and instead the homogenized transport equation is determined by integrating the $\mathcal{O}(\varepsilon)$ system over Ω_c. Equating coefficients of ε^0 gives

$$\mathcal{L}_1 c_c^{(0)} = 0 \quad \text{in } \Omega_c, \tag{101}$$

$$A_c\nabla_X c_c^{(0)}\cdot\mathbf{n} = 0 \quad \text{on } \Gamma_\epsilon, \tag{102}$$

and so the leading-order capillary concentration, $c_c^{(0)} = \bar{c}(\mathbf{x},t)$, is locally uniform. Equating coefficients of ε^1 gives

$$\mathcal{L}_1 c_t^{(0)} = 0 \quad \text{in } \Omega_t, \tag{103}$$

$$c_t^{(0)} = \overline{c} \quad \text{on } \Gamma_\epsilon, \tag{104}$$

$$\mathcal{L}_1 c_c^{(1)} = \frac{\partial\overline{c}}{\partial t} + \left(\mathbf{u}_c^{(0)}\cdot\nabla_x\right)\overline{c} \quad \text{in } \Omega_c, \tag{105}$$

$$A_c\nabla_X c_c^{(1)}\cdot\mathbf{n} = \left(A_t\nabla_X c_t^{(0)} - A_c\nabla_x\overline{c} + \bar{c}\mathbf{u}_c^{(1)}\right)\cdot\mathbf{n} \quad \text{on } \Gamma_\epsilon, \tag{106}$$

which is a Dirichlet problem for the leading-order interstitial concentration $c_t^{(0)}$, and a Neumann problem for the correction term in the capillaries, $c_c^{(1)}$. We use separation of variables to solve for $c_t^{(0)}$ by setting $c_t^{(0)} = \overline{c}(\mathbf{x},t)g(\mathbf{X})$; g represents the local variation in the species concentration in the interstitium due to uptake, and is determined through the cell problem

$$\mathcal{L}_1 g = 0 \quad \text{in } \Omega_t, \tag{107}$$

$$g = 1 \quad \text{on } \Gamma_\epsilon. \tag{108}$$

By integrating (107) over Ω_t, we find

$$\frac{A_t}{|\Omega_t|}\int_{\Gamma_\epsilon}\nabla_X g\cdot\mathbf{n}\,\mathrm{d}S = -\mathrm{Da}\langle g\rangle_t, \tag{109}$$

and so the local flux of species into the interstitium balances with that lost by reaction. Integrating (105) over Ω_c gives

$$\frac{A_c}{|\Omega_c|}\int_{\Gamma_\epsilon}\nabla_X c_c^{(1)}\cdot\mathbf{n}\,\mathrm{d}S=\frac{\partial\overline{c}}{\partial t}+\left\langle\mathbf{u}_c^{(0)}\right\rangle_c\cdot\nabla_x\overline{c}. \tag{110}$$

Now using (106) and (109) together with the divergence theorem to evaluate the left-hand side of (110) gives

$$\begin{aligned}\frac{A_c}{|\Omega_c|}\int_{\Gamma_\epsilon}\nabla_X c_c^{(1)}\cdot\mathbf{n}\,\mathrm{d}S&=\frac{1}{|\Omega_c|}\int_{\Gamma_\epsilon}\overline{c}\mathbf{u}_c^{(1)}\cdot\mathbf{n}\,\mathrm{d}S-\frac{\mathrm{Da}\,n_t}{n_c}\langle g\rangle_t\overline{c}\\&=\frac{\overline{c}}{|\Omega_c|}\int_{\Omega_c}\nabla_X\cdot\mathbf{u}_c^{(1)}\,\mathrm{d}V-\frac{\mathrm{Da}\,n_t}{n_c}\langle g\rangle_t\overline{c}\\&=-\overline{c}\nabla_x\cdot\left\langle\mathbf{u}_c^{(0)}\right\rangle_c-\frac{\mathrm{Da}\,n_t}{n_c}\langle g\rangle_t\overline{c}.\end{aligned} \tag{111}$$

This yields the transport equation

$$n_c\left(\frac{\partial\overline{c}}{\partial t}+\nabla_x\cdot\left(\left\langle\mathbf{u}_c^{(0)}\right\rangle_c\overline{c}\right)\right)=-\mathrm{Da}\,n_t\langle g\rangle_t\overline{c}. \tag{112}$$

In this case, the average tracer concentration is given by

$$\hat{c}=n_c\langle c_c\rangle_c+n_t\langle c_t\rangle_t=n_c\overline{c}(\mathbf{x},t)+\mathcal{O}(\varepsilon), \tag{113}$$

and consequently, the transport of $\hat{c}$ is also described by Eq. (112). The species is advected by the average fluid velocity in the capillaries and also reacts due to due decay/metabolism, as represented by the term $-\mathrm{Da}\langle g\rangle_t\overline{c}$.

3.2.3. Weak reaction and continuity of concentration on Γ_ϵ

Next, we consider the case when $\mathrm{Da}=\mathcal{O}(\varepsilon)$ and $D_r=\mathcal{O}(1)$, together with continuity of concentration and flux boundary conditions on Γ_ϵ. We define the $\mathcal{O}(1)$ parameter $\overline{\mathrm{Da}}$ through $\mathrm{Da}=\varepsilon\,\overline{\mathrm{Da}}$, and let

$$\bar{\mathcal{R}}=\begin{cases}0 & \text{in } \Omega_c,\\ \overline{\mathrm{Da}} & \text{in } \Omega_t.\end{cases} \tag{114}$$

Then

$$\varepsilon\frac{\partial c}{\partial t}+\varepsilon\nabla_x\cdot(c\mathbf{u})+\nabla_X\cdot(c\mathbf{u})=A\nabla_X^2c+2A\varepsilon\nabla_x\cdot\nabla_Xc+\varepsilon^2A\nabla_x^2c-\varepsilon\overline{\mathcal{R}}c\quad\text{in }\Omega, \tag{115}$$

with the two continuity boundary conditions (79) and (80) on Γ. This system is similar to the tracer system of Section 3.2.1, although reaction through $\overline{\mathrm{Da}}$ contributes to the $\mathcal{O}(\varepsilon)$ system. The systems in Ω_c and Ω_t are coupled at each order so the homogenized transport equation will be derived using the invariant distribution approach. The $\mathcal{O}(1)$

system is unchanged from the tracer transport problem (83) with boundary conditions (84) and so $c^{(0)} = \overline{c}(\mathbf{x}, t)$ is locally uniform across Ω. We introduce the same stationary invariant distribution $\rho = 1/|\Omega|$. The $\mathcal{O}(\varepsilon)$ system is given by

$$\mathcal{L}_0 c^{(1)} = \frac{\partial \overline{c}}{\partial t} + \left(\mathbf{u}^{(0)} \cdot \nabla_x\right)\overline{c} + \bar{\mathcal{R}}\overline{c} \quad \text{in } \Omega, \tag{116}$$

$$c_c^{(1)} = c_t^{(1)} \quad \text{and} \quad \left(A_c \nabla_X c_c^{(1)} - A_t \nabla_X c_t^{(1)}\right) \cdot \mathbf{n} = (A_t - A_c)\nabla_x \overline{c} \cdot \mathbf{n} \quad \text{on } \Gamma_\epsilon. \tag{117}$$

The solvability condition for this system is obtained by averaging over the whole domain Ω to give

$$\frac{\partial \overline{c}}{\partial t} + \nabla_x \cdot \left(\tilde{\mathbf{u}}^{(0)}\overline{c}\right) = -\overline{\mathrm{Da}}\, n_t \overline{c}, \tag{118}$$

where $\tilde{\mathbf{u}}^{(0)}$ is the combined fluid velocity in the capillaries and tissue given by (92). The average species concentration is given by $\hat{c} = \overline{c} + \mathcal{O}(\varepsilon)$ and, therefore, also satisfies the transport equation (118).

3.2.4. Weak reaction with a membrane law on Γ_ϵ

We consider the case when $\mathrm{Da} = \mathcal{O}(\varepsilon)$ together with $D_r = \mathcal{O}(1)$, and use the membrane law description of the boundary given by (31). The system equations are therefore given by (115), however, the boundary conditions on Γ_ϵ change to

$$(c_c \mathbf{u}_c - A_c \nabla_X c_c - \varepsilon A_c \nabla_x c_c) \cdot \mathbf{n} = (c_t \mathbf{u}_t - A_t \nabla_X c_t - A_t \varepsilon \nabla_x c_t) \cdot \mathbf{n} \tag{119}$$

$$= \varepsilon \overline{\Upsilon}(c_c - c_t). \tag{120}$$

The species concentrations in the capillaries and interstitium are both $\mathcal{O}(1)$; performing multiple-scales expansions of the form (78) yields the $\mathcal{O}(1)$ system

$$\mathcal{L}_0 c^{(0)} = 0 \quad \text{in } \Omega, \tag{121}$$

$$A_c \nabla_X c_c^{(0)} \cdot \mathbf{n} = A_t \nabla_X c_t^{(0)} \cdot \mathbf{n} = 0 \quad \text{on } \Gamma_\epsilon. \tag{122}$$

Therefore, $c_c^{(0)} = \overline{c}_c(\mathbf{x}, t)$ and $c_t^{(0)} = \overline{c}_t(\mathbf{x}, t)$ are both locally uniform. However, the change in boundary condition to the membrane approach means that $\overline{c}_c$ and $\overline{c}_t$ are no longer equal on the internal boundary Γ_ϵ. We must therefore determine two homogenized equations to describe the average concentration in each of the capillaries and interstitium. The $\mathcal{O}(\varepsilon)$ system is given by

$$\mathcal{L}_0 c^{(1)} = \frac{\partial c^{(0)}}{\partial t} + \mathbf{u}^{(0)} \cdot \nabla_x c^{(0)} + \bar{\mathcal{R}} c^{(0)} \quad \text{in } \Omega, \tag{123}$$

$$A_c \nabla_X c_c^{(1)} \cdot \mathbf{n} = \overline{c}_c \mathbf{u}_c^{(1)} \cdot \mathbf{n} - A_c \nabla_x \overline{c}_c \cdot \mathbf{n} - \bar{\Upsilon}(\overline{c}_c - \overline{c}_t) \quad \text{on } \Gamma_\epsilon, \tag{124}$$

$$A_t \nabla_X c_t^{(1)} \cdot \mathbf{n} = \overline{c}_t \mathbf{u}_t^{(1)} \cdot \mathbf{n} - A_t \nabla_x \overline{c}_t \cdot \mathbf{n} - \bar{\Upsilon}(\overline{c}_c - \overline{c}_t) \quad \text{on } \Gamma_\epsilon. \tag{125}$$

The systems in Ω_c and Ω_t decouple, therefore, we derive the leading-order homogenized transport equations by averaging over Ω_c or Ω_t, respectively, to give

$$\frac{\partial \overline{c}_c}{\partial t} + \nabla_x \cdot \left(\langle \mathbf{u}_c^{(0)} \rangle_c \overline{c}_c \right) = -\frac{\bar{\Upsilon} S}{|\Omega_c|} (\overline{c}_c - \overline{c}_t), \tag{126}$$

$$\frac{\partial \overline{c}_t}{\partial t} + \nabla_x \cdot \left(\langle \mathbf{u}_t^{(0)} \rangle_t \overline{c}_t \right) = -\overline{\mathrm{Da}}\, \overline{c}_t + \frac{\bar{\Upsilon} S}{|\Omega_t|} (\overline{c}_c - \overline{c}_t). \tag{127}$$

Equation (126) represents the transport of the leading-order average species concentration in the capillaries, whilst Eq. (127) represents that in the interstitium; both are advection–reaction equations describing the respective concentrations. Transport of total average species concentration $\langle c \rangle = n_c \langle c_c \rangle_c + n_t \langle c_t \rangle_t$ is therefore described by

$$\frac{\partial}{\partial t} (n_c \overline{c}_c + n_t \overline{c}_t) + \nabla_x \cdot \left(\overline{c}_c n_c \langle \mathbf{u}_c^{(0)} \rangle_c + \overline{c}_t n_t \langle \mathbf{u}_t^{(0)} \rangle_t \right) = -\overline{\mathrm{Da}}\, n_t \overline{c}_t. \tag{128}$$

3.2.5. Weak reaction with a jump in diffusivities across Γ_ϵ and membrane law
Finally, we consider the case when reaction is weak in the interstitium so that $\mathrm{Da} = \mathcal{O}(\varepsilon)$, together with a jump in diffusivities across Γ_ϵ so that $D_r = \mathcal{O}(\varepsilon)$. We also use the membrane form of boundary condition on Γ_ϵ, given in dimensionless form by (31).

Given that $D_r = \mathcal{O}(\varepsilon)$, the diffusion coefficient in the interstitium is $\mathcal{O}(\varepsilon)$. It is unlikely that advection is the dominant transport mechanism locally, and therefore we consider the case when the fluid velocity in the interstitium, $\mathbf{u}_t$, is also $\mathcal{O}(\varepsilon)$, so that the local Péclet number remains $\mathcal{O}(1)$. We capture this change by maintaining the ratio $\phi = \mathcal{O}(\varepsilon^2)$, but applying the scalings $\kappa = \mathcal{O}(1)$ and $R = \mathcal{O}(\varepsilon^2)$, thereby reducing the order of magnitude of both the interstitial and vascular permeability by an order ε. This is equivalent to taking the limit $\overline{R} \to 0$ with $\overline{\psi}$ fixed in the pressure Eqs. (54) and (75). This leaves the equation for the interstitial fluid pressure (54) unchanged, but the leading-order capillary fluid pressure equation becomes

$$\nabla_x \cdot \left(\mathbf{K} \nabla_x p_c^{(0)} \right) = 0. \tag{129}$$

In addition, the capillary fluid velocity given by (70) is unchanged, whilst the interstitial fluid velocity is an order of magnitude smaller. We set

$$\mathbf{u}_t = \varepsilon \hat{\mathbf{u}}_t, \tag{130}$$

where the leading-order term $\langle \hat{\mathbf{u}}_t^{(0)} \rangle_t$ is given by

$$\left\langle \hat{\mathbf{u}}_t^{(0)} \right\rangle_t = -\kappa \mathbf{E} \cdot \nabla_x p_t^{(0)}. \tag{131}$$

It should be noted that when $\kappa = kL/d^3 = \mathcal{O}(1)$, then $k = \mathcal{O}(\varepsilon d^2)$ and so $\phi = \alpha d/\sqrt{k} = \mathcal{O}(\alpha/\sqrt{\varepsilon})$. Therefore, given experimentally determined $\alpha = \mathcal{O}(1)$, the Beavers–Joseph boundary condition may be approximated by a no-slip boundary condition at leading order.

We define $\hat{D}_r = D_r/\varepsilon = \mathcal{O}(1)$ with $\hat{A}_t = \hat{D}_r/\mathrm{Pe}_l$, and non-dimensionalize all variables with their respective scales in Ω_c and Ω_t separately. The system equations are then given

by

$$\varepsilon\frac{\partial c_c}{\partial t}+\varepsilon\nabla_x\cdot(c_c\mathbf{u}_c)+\nabla_X\cdot(c_c\mathbf{u}_c)=A_c\nabla_X^2c_c+2A_c\varepsilon\nabla_x\cdot\nabla_Xc_c$$
$$+\varepsilon^2A_c\nabla_x^2c_c\quad\text{in }\Omega_c,\tag{132}$$
$$\varepsilon\frac{\partial c_t}{\partial t}+\varepsilon\nabla_x\cdot(c_t\mathbf{u}_t)+\nabla_X\cdot(c_t\mathbf{u}_t)=\hat{A}_t\nabla_X^2c_t+2\hat{A}_t\varepsilon\nabla_x\cdot\nabla_Xc_t+\varepsilon^2\hat{A}_t\nabla_x^2c_t$$
$$-\overline{\mathrm{Da}}\,c_t\quad\text{in }\Omega_t,\tag{133}$$

with boundary conditions on Γ_ϵ given by

$$(c_c\mathbf{u}_c-A_c\nabla_Xc_c-\varepsilon A_c\nabla_xc_c)\cdot\mathbf{n}=\left(\varepsilon c_t\hat{\mathbf{u}}_t-\varepsilon\hat{A}_t\nabla_Xc_t-\varepsilon^2\hat{A}_t\nabla_xc_t\right)\cdot\mathbf{n}\tag{134}$$
$$=\varepsilon\overline{\Upsilon}(c_c-c_t).\tag{135}$$

The species concentration in both the capillaries and interstitium is $\mathcal{O}(1)$, therefore, we employ multiple-scales expansions of the form (78) together with

$$\mathbf{u}_c=\mathbf{u}_c^{(0)}+\varepsilon\mathbf{u}_c^{(1)}+\cdots,\tag{136}$$
$$\hat{\mathbf{u}}_t=\hat{\mathbf{u}}_t^{(0)}+\varepsilon\hat{\mathbf{u}}_t^{(1)}+\cdots.\tag{137}$$

We define the operator

$$\mathcal{L}_2\star:=\begin{cases}A_c\nabla_X^2\star-\nabla_X\cdot(\mathbf{u}_c^{(0)}\star) & \text{in }\Omega_c,\\ \hat{A}_t\nabla_X^2\star-\nabla_X\cdot(\hat{\mathbf{u}}_t^{(0)}\star)-\overline{\mathrm{Da}}\star & \text{in }\Omega_t,\end{cases}\tag{138}$$

equipped with periodic boundary conditions on Ω. The $\mathcal{O}(1)$ system is

$$\mathcal{L}_2c^{(0)}=0,\tag{139}$$

together with the boundary conditions

$$-A_c\nabla_Xc_c^{(0)}\cdot\mathbf{n}=0,\tag{140}$$
$$-\hat{A}_t\nabla_Xc_t^{(0)}\cdot\mathbf{n}=\overline{\Upsilon}\left(c_c^{(0)}-c_t^{(0)}\right),\tag{141}$$

on Γ_ϵ. The system decouples; the leading-order species concentration in the capillaries is locally uniform and denoted $\overline{c}(\mathbf{x},t)$. The leading-order species concentration in the interstitium is then the solution to the Robin problem

$$\mathcal{L}_2c_t^{(0)}=0\quad\text{in }\Omega_t,\tag{142}$$
$$\overline{\Upsilon}c_t^{(0)}-\hat{A}_t\nabla_Xc_t^{(0)}\cdot\mathbf{n}=\overline{\Upsilon}\overline{c}(\mathbf{x},t)\quad\text{on }\Gamma_\epsilon.\tag{143}$$

We separate $c_t^{(0)}$ into globally and locally varying components by setting

$$c_t^{(0)}=\overline{c}(\mathbf{x},t)h(\mathbf{X}).\tag{144}$$

The locally varying component $h(\mathbf{X})$ is the solution to the cell problem

$$\mathcal{L}_2 h = 0 \quad \text{in } \Omega_t, \tag{145}$$

$$\overline{\Upsilon} h - \hat{A}_t \nabla_X h \cdot \mathbf{n} = \overline{\Upsilon} \quad \text{on } \Gamma_\epsilon. \tag{146}$$

The component $\overline{c}(\mathbf{x}, t)$ is determined from a homogenized equation that is derived from the $\mathcal{O}(\varepsilon)$ system in Ω_c, which now reduces to

$$\mathcal{L}_2 c_c^{(1)} = \frac{\partial \overline{c}}{\partial t} + \left(\mathbf{u}_c^{(0)} \cdot \nabla_x\right)\overline{c} \quad \text{in } \Omega_c, \tag{147}$$

$$A_c \nabla_X c_c^{(1)} \cdot \mathbf{n} = \overline{c}\mathbf{u}_c^{(1)} \cdot \mathbf{n} + \overline{\Upsilon}\overline{c}(h-1) - A_c \nabla_x \overline{c} \cdot \mathbf{n} \quad \text{on } \Gamma_\epsilon. \tag{148}$$

Integrating over Ω_c and using the cell problem for h given by (145)–(146) together with $\hat{\mathbf{u}}_t^{(0)} = 0$ on Γ_ϵ yields the homogenized equation

$$n_c\left(\frac{\partial \overline{c}}{\partial t} + \nabla_x \cdot \left(\left\langle \mathbf{u}_c^{(0)} \right\rangle_c \overline{c}\right)\right) = -\overline{\mathrm{Da}}\, n_t \langle h \rangle_t \overline{c}. \tag{149}$$

The average species concentration is given by

$$\hat{c} = n_c \langle c_c \rangle_c + n_t \langle c_t \rangle_t = \overline{c}\left(n_c + n_t \langle h \rangle_t\right) + \mathcal{O}(\varepsilon), \tag{150}$$

and may be evaluated by solving the effective Eq. (149). This is the only one of our examples where the local variation in species concentration impacts the leading-order transport equation.

4. Discussion

Let us summarise the five models we have derived. In particular, let us look at the structure of the equations in each case.

The simplest equations arise in cases 1 and 3. There the concentration c is the same in the capillaries and interstitium at leading order and the reaction–convection equation takes the form

$$\frac{\partial c}{\partial t} + \nabla \cdot (\mathbf{u}c) = -\mathcal{R}c, \tag{151}$$

where $\mathbf{u}$ is the average of the interstitial and capillary fluid velocities. In case 1, the reaction term is absent.

A similar equation holds in cases 2 and 4, but now most of the convection takes place in the capillaries, and $\mathbf{u}$ is the capillary fluid velocity. The concentrations in the capillaries and interstitium are no longer equal, and c represents some weighted average concentration.

Finally, in case 5, both capillary and interstitial concentrations need to be tracked independently, giving

$$\frac{\partial c_c}{\partial t} + \nabla \cdot (\mathbf{u}_c c_c) = -K(c_c - c_t), \tag{152}$$

$$\frac{\partial c_t}{\partial t} + \nabla \cdot (\mathbf{u}_t c_t) = K(c_c - c_t) - \mathcal{R}c_t, \tag{153}$$

where K gives the transfer from capillaries to the interstitium.

It is rare that the transport properties of anti-cancer agents are fully characterized, and as a consequence data on only a small proportion of the agents available clinically are presented in this paper. Of these, [^{14}C]-sucrose, [^{3}H]-vinblastine, TPZ (V79–171b MCLs) (oxic) and TPZ (MGH–U1 MCLs) (oxic) are tracers and follow case 1. Therefore, for these agents the concentration is the same in the capillaries and interstitium at leading order, and this concentration follows Eq. (151) (with no reaction term). By comparison, [^{14}C]-Pt(II), [^{14}C]-Pt(IV), TPZ, TPZ Analogue 3, TPZ Analogue 10, TPZ (V79–171b MCLs) (anoxic) and TPZ (MGH–U1 MCLs) (anoxic) follow case 5. Therefore, both the capillary and interstitial concentrations should be tracked independently, according to Eqs. (152)–(153).

The final models (151), (152)–(153) can now be solved alongside the fluid transport equations to investigate how vascular structure impacts on drug delivery. First of all, the fluid perfusion equations should be solved on a tumour domain (provided by a medical image), as described at the end of Section 3.1. This will determine the advecting velocities in Eqs. (151) and (152)–(153), which can now be solved on the same tumour domain subject to Dirichlet or Neumann boundary conditions to mimic the drug delivery mechanism. For example, for an injection of the drug a Dirichlet condition that mimics the concentration of drug delivered to the tumour should be applied. However, for constant perfusion of a drug over a fixed time period a Neumann flux condition should be applied.

5. Diffusion

Equations (94), (112), (118), (126)–(127), and (149) are the leading-order homogenized species transport equations for the five physiological cases identified in Section 3.2. These are advection–reaction equations; they do not include diffusion which features on an $\mathcal{O}(1/\varepsilon)$ time scale globally, and thus contributes an $\mathcal{O}(\varepsilon)$ correction to the leading-order equations derived in this paper. Although these $\mathcal{O}(\varepsilon)$ corrections are not included here, they can be readily evaluated as detailed in Shipley (2008). Firstly, the $\mathcal{O}(\varepsilon)$ contributions to the species concentration, $c^{(1)}$, must be determined by using the homogenized equations to eliminate time derivative terms from the system description of $c^{(1)}$ (for example, for tracer transport, by using Eq. (94) to eliminate $\partial\overline{c}/\partial t$ terms from the system (85)). We then solve for $c^{(1)}$ by exploiting linearity, and decomposing the solution into locally and globally varying components (the locally varying parts are determined from various micro-scale cell problems, as in the fluid transport problem). Finally, integrating the system determined by equating coefficients of ε^2, yields the $\mathcal{O}(\epsilon)$ corrections, including diffusion, to the homogenized transport equations presented here.

6. Conclusion

We have developed theoretical models that describe the transport of fluid and drugs in solid tumours through both the vascular and the interstitial compartments, and at a number

of length scales. We started by posing the transport problems on the length scale characterized by the inter-capillary separation, and classified pertinent scalings regimes through the process of non-dimensionalization and parameter estimation. We then used multiple scales to form continuum models describing fluid and drug transport that corresponded to each of the scaling regimes identified.

The resulting fluid equations form a double porous medium; both the vascular network and the tumour interstitium behave as a porous media, with fluid transport between them. This generalized the model of Chapman et al. (2008) to an arbitrary (periodic) vascular configuration, and provides a mechanism for testing the impact of vascular structure on fluid perfusion in tumours.

The continuum drug equations comprise advection–reaction equations, where the advection and reaction coefficients are dependent on the scaling regime under investigation, and the vascular morphology. We considered five different regimes, characterized by the importance of reaction, interstitial diffusion, and the boundary condition on the capillary wall. For four of these regimes, an appropriate average drug concentration satisfies an advection–reaction equation, with the advection velocity and reaction term depending on the particular regime considered. In the final case the interstitial and capillary concentration both need to be tracked independently leading to two coupled reaction–advection equations.

Although the motivation for this work is transport in tumours, the approach can be readily generalized to healthy tissue. Indeed, the key physiological difference (other than vascular structure) is a lower vascular permeability in healthy tissue; the impact of this can be explored through the limiting case $\overline{R} \to 0$ (with $\overline{\kappa}$ fixed) in the homogenized fluid transport equations (54) and (75). This results in decoupled homogenized equations for p_c and p_t given by

$$\nabla_x \cdot \left(\mathbf{E} \cdot \nabla_x p_t^{(0)}\right) = 0, \qquad \nabla_x \cdot \left(\mathbf{K} \cdot \nabla_x p_c^{(0)}\right) = 0. \tag{154}$$

In this way, the models presented here can be used to investigate fluid perfusion and drug distribution in a wide range of tissues.

The model we have presented makes several simplifying assumptions and is open to improvement in a number of areas. The regularity of a periodic micro-structure is not necessarily representative of the tumour vasculature, and does not account for temporal changes in vascular structure due to re-modelling or adaption. It would be an interesting and challenging extension of the model to extend this homogenization technique to account for these factors. Further, the blood in the microcirculation does not indeed behave as a Newtonian fluid, but rather is a shear-thinning fluid with a haematocrit-dependent viscosity. It is important that future work should take account of microvascular rheology in a more realistic way.

Finally, although this paper is focussed on theoretical model development, the next natural step is to simulate the continuum models of fluid and drug transport derived here on tumour geometries provided by medical images. This will allow both model validation (by comparison against clinical data), and the use of model predictions to elucidate the connection between blood and mass transport and vascular structure.

References

Arbogast, T., Douglas, J., Hornung, U., 1990. Derivation of the double porosity model of single phase flow via homogenization theory. SIAM J. Math. Anal. 21, 823–836.

Arbogast, T., Douglas, J., Hornung, U., 1991. Modeling of naturally fractured reservoirs by formal homogenization techniques. In: Frontiers in Pure and Applied Mathematics, pp. 1–19. Elsevier, Amsterdam.

Arbogast, T., Lehr, H., 2006. Homogenization of a Darcy–Stokes system modeling vuggy porous media. Comput. Geosci. 10, 291–302.

Beavers, G., Joseph, D., 1967. Boundary conditions at a naturally permeable wall. J. Fluid Mech. 30, 197–207.

Cameliet, P., Jain, R., 2000. Angiogenesis in cancer and other diseases. Nature 407, 249–257.

Chapman, S., Shipley, R., Jawad, R., 2008. Multiscale modeling of fluid transport in tumors. Bull. Math. Biol. 70, 2334–2357.

Fåhraeus, R., 1928. Die strölmungsverhältnisse und die verteilung der blutzellen im gefäbsystem. Zur frage der bedeutung der intravasculären erythrocytenaggregation. Klin. Wochenschr. 7, 100–106.

Fåhraeus, R., Lindqvist, T., 1931. The viscosity of the blood in narrow capillary tubes. Am. J. Physiol. 96, 562–568.

Hashizume, H., Baluk, P., Morikawa, S., McLean, J., Thurston, G., Roberge, S., Jain, R., McDonald, D., 2000. Openings between defective endothelial cells explain tumor vessel leakiness. Am. J. Pathol. 156, 1363–1380.

Heldin, C., Rubin, K., Pietras, K., Ostman, A., 2004. A high interstitial fluid pressure—an obstacle in cancer therapy. Nat. Rev. Cancer 4, 806–813.

Hicks, K., Fleming, Y., Siim, B., Koch, C., Wilson, W., 1998. Extravascular diffusion of tirapazamine: Effect of metabolic consumption assessed using the multicellular layer model. Int. J. Radiat. Oncol. Biol. Phys. 42, 641–649.

Hicks, K., Pruijn, F., Secomb, T.W., Hay, M., Hsu, R.H., Brown, J., Denny, W., Dewhirst, M., Wilson, W., 2006. Use of three-dimensional tissue cultures to model extravascular transport and predict In vivo activity of hypoxia-targeted anticancer drugs. J. Nat. Cancer Inst. 98, 1118–1128.

Intaglietta, M., Silverman, N., Tompkins, W., 1975. Capillary flow velocity in vivo and in situ by television methods. Microvasc. Res. 10, 165–179.

Jäger, W., Mikelić, A., 2000. On the interface boundary conditions by Beavers, Joseph and Saffman. SIAM J. Appl. Math. 60, 1111–1127.

Jäger, W., Mikelić, A., Neuss, M., 2001. Asymptotic analysis of the laminar viscous flow over a porous bed. SIAM J. Sci. Comput. 22, 2006–2028.

Jain, R., 1987. Transport of molecules across tumor vasculature. Cancer Metastasis Rev. 6, 559–593.

Jain, R., 1989. Delivery of novel therapeutic agents in tumors: physiological barriers and strategies. J. Natl. Cancer Inst. 81(8), 570–576.

Jain, R., 1990. Vascular and interstitial barriers to delivery of therapeutic agents in tumors. Cancer Metastasis Rev. 9, 253–266.

Jang, S., Wientjies, M., Lu, D., Au, J., 2003. Drug delivery and transport to solid tumors. Pharm. Res. 20, 1337–1350.

Jones, I., 1973. Low Reynolds number flow past a porous spherical shell. Proc. Camb. Philos. Soc. 73, 231–238.

Kenner, T., 1989. The measurement of blood density and its meaning. Basic Res. Cardiol. 84, 111–124.

Kirkpatrick, J., Brizel, D.M., Dewhirst, M., 2003. A mathematical model of tumor oxygen and glucose mass transport and metabolism with complex reaction kinetics. Radiat. Res. 159, 336–344.

Konerding, M., Malkusch, W., Klapthor, B., Van Ackern, C., Fait, E., Hill, S., Parkins, C., Chaplin, D., Presta, M., Denekamp, J., 1999. Evidence for characteristic vascular patterns in solid tumours: Quantitative studies using corrosion casts. Br. J. Cancer 80, 724.

Konerding, M., Fait, E., Gaumann, A., et al., 2001. 3D microvascular architecture of pre-cancerous lesions and invasive carcinomas of the colon. Br. J. Cancer 84, 1354–1362.

Less, J., Skalak, T., Sevick, E., Jain, R., 1991. Microvascular architecture in a mammary carcinoma: Branching patterns and vessel dimensions. Cancer Res. 51, 265–273.

Minchinton, A.I., Tannock, I.F., 2006. Drug penetration in solid tumours. Nat. Rev. Cancer 6(8), 583–592.

Modok, S., Hyde, P., Mellor, H., Roose, T., Callaghan, R., 2006. Diffusivity and distribution of vinblastine in three-dimensional tumour tissue: Experimental and mathematical modelling. Eur. J. Cancer 42, 2404–2413.

Modok, S., Scott, R., Alderden, R., Hall, M., Mellor, H., Bohic, S., Roose, T., Hambley, T., Callaghan, R., 2007. Transport kinetics of four-and six-coordinate platinum compounds in the multicell layer tumour model. Br. J. Cancer 97, 194–200.

Pries, A., Secomb, T., 2005. Microvascular blood viscosity in vivo and the endothelial surface layer. Am. J. Physiol. Heart Circ. Physiol. 289, H2657–H2664.

Pries, A., Ley, K., Claassen, M., Gaehtgens, P., 1989. Red cell distribution at microvascular bifurcations. Microvasc. Res. 38, 81–101.

Pries, A., Neuhaus, D., Gaehtgens, P., 1992. Blood viscosity in tube flow: Dependence on diameter and hematocrit. Am. J. Physiol. 263, H1770–H1778.

Pries, A., Cornelissen, A., Sloot, A., Hinkeldey, M., Dreher, M., Höpfner, M., Dewhirst, M., Secomb, T., 2009. Structural adaptation and heterogeneity of normal and tumor microvascular networks. PLoS Comput. Biol. 5.

Rand, P., Lacombe, E., Hunt, H., Austin, W., 1964. Viscosity of normal human blood under normothermic and hypothermic conditions. J. Appl. Physiol. 19, 117–122.

Saffman, P., 1971. On the boundary condition at the surface of a porous medium. Stud. Appl. Math. I, volume 2, 93–101.

Shipley, R.J., 2008. Multiscale modelling of fluid and drug transport in vascular tumours. PhD thesis, University of Oxford.

Yao, D., Ding, S., Burchell, B., Wolf, C.R., Friedberg, T., 2000. Detoxication of vinca alkaloids by human P450 CYP3A4-mediated metabolism: Implications for the development of drug resistance. J. Pharmacol. Exp. Ther. 294, 387–395.